Vesicle Migration and Spatial Organization Driven by Flow Line Curvature

Giovanni Ghigliotti,[1] Abtin Rahimian,[2] George Biros,[2] and Chaouqi Misbah[1]

[1]*Université Joseph Fourier and CNRS (UMR5588), Laboratoire de Spectrométrie Physique, 140 Avenue de la Physique, 38402 Saint Martin d'Hères, France*

[2]*Georgia Institute of Technology, School of Computational Science and Engineering and Department of Biomedical Engineering, 1324 Klaus Advanced Computing Building, 266 Ferst Drive, Atlanta, Georgia 30332-0765, USA*

(Received 22 October 2010)

Cross-streamline migration of deformable entities is essential in many problems such as industrial particulate flows, DNA sorting, and blood rheology. Using two-dimensional numerical experiments, we have discovered that vesicles suspended in a flow with curved flow lines migrate towards regions of high flowline curvature, which are regions of high shear rates. The migration velocity of a vesicle is found to be a universal function of the normal stress difference and the flow curvature. This finding quantitatively demonstrates a direct coupling between a microscopic quantity (migration) and a macroscopic one (normal stress difference). Furthermore, simulations with multiple vesicles revealed a self-organization, which corresponds to segregation, in a rim closer to the inner cylinder, resulting from a subtle interaction among vesicles. Such segregation effects could have a significant impact on the rheology of vesicle flows.

DOI: PACS numbers: 87.16.D−, 83.50.Ha, 83.80.Iz, 87.17.Jj

Introduction.—Complex fluids are generally made of rigid or soft particles that are suspended in a Newtonian fluid. Examples of complex fluids include emulsions, polymer solutions, particulate suspensions (many food products belong to this category), and blood. One of the major challenges in understanding the physics of complex fluids is the link between the local microstructure (i.e., spatiotemporal organization of suspended entities) and the macroscopic rheology. Microstructures spontaneously arise in many complex fluids, and may have a dramatic impact on flow properties [1].

A phenomenon that may induce inhomogeneous organization of the suspended entities is lateral or cross-streamline migration. Recall that a single rigid spherical particle immersed in a Newtonian fluid at vanishing Reynolds number Re cannot migrate in the direction transverse to the flow lines [2]. On the contrary, deformable particles have the ability to migrate cross-streamline, even at $\mathrm{Re} = 0$—if a certain symmetry is broken, for example, the centrosymmetry in linear shear flow. Symmetries may be broken due to the presence of walls, gradient in shear rate (e.g., Poiseuille flow), or the presence of flowline curvature (e.g., cylindrical Couette flow).

Cross-streamline migration appears in many applications, such as industrial polymer processing [3], DNA sorting [4], drop dynamics [5], and biofluids. A prominent example of the latter system is blood flow in which cross-streamline migration of erythrocytes may result in decreased blood viscosity, reducing blood flow resistance in microvasculature (Fåhræus-Lindqvist effect).

A common belief is that deformable particles have the tendency to migrate towards regions of low shear rates [6–10]. In some circumstances, however, the opposite is predicted (the case of drops in a certain range of viscosity contrast between the internal an external fluids [5]). In this Letter, we propose an explanation for these differences and provide quantitative evidence for the case of vesicle flows. Our discussion will allow us to conjecture general principles that can be used to predict lateral migration. The study of multiple vesicles reveals a self-organization in a rim.

We carried out simulations in a Taylor-Couette cell by taking vesicles as a model system for the suspended entities. Vesicles are liquid drops delimited by a lipid bilayer [11–13]; they constitute a simple model for the description of some features of red blood cell dynamics. We have chosen to simulate the Taylor-Couette system because it is widely used for studying the rheology of complex fluids.

Methods.—The numerical simulations are carried out in two dimensions using a boundary integral formulation. For simplicity, here we state the free-space formulation (the formulation for confined flows can be found in [14]):

$$\begin{aligned}\mathbf{v}(\mathbf{x}_0) = {} & \frac{2}{1+\lambda}\mathbf{v}^{\infty}(\mathbf{x}_0) \\ & + \frac{1}{2\pi\eta_0(1+\lambda)}\oint_{\gamma} G(\mathbf{x}-\mathbf{x}_0)\cdot\mathbf{f}(\mathbf{x})ds(\mathbf{x}) \\ & + \frac{2(1-\lambda)}{\pi(1+\lambda)}\oint_{\gamma}\mathbf{v}(\mathbf{x})\cdot T(\mathbf{x}-\mathbf{x}_0)\cdot\mathbf{n}(\mathbf{x})ds(\mathbf{x}), \quad (1)\end{aligned}$$

where γ is the vesicle membrane, $\mathbf{v}$ the membrane velocity, G and T the Green's functions of the Stokes flow, $\mathbf{x}_0$ and $\mathbf{x}$ are points on the vesicle membrane, $\mathbf{f}$ is the membrane force, $\mathbf{n}$ the outward normal to the membrane, η_0 the viscosity of the suspending fluid, and $\lambda = \eta_1/\eta_0$ the viscosity contrast between the internal and the external fluids. The membrane force has contributions from bending energy and local inextensibility [15,16]:

$$\mathbf{f}(\mathbf{x}) = -\kappa\left[\frac{d^2c}{ds^2} + \frac{1}{2}c^3\right]\mathbf{n} + \zeta c\mathbf{n} + \frac{d\zeta}{ds}\mathbf{t}, \qquad (2)$$

where κ is the bending modulus, c the membrane curvature, ζ a local Lagrange multiplier enforcing membrane inextensibility, and $\mathbf{t}$ the normalized tangent to the membrane. For the single-vesicle free-space case, we used two implementations; the first one is detailed in [17]; the second one, which was also used for multiple vesicles and confined flows, is detailed in [14]. Both implementations give the same dynamics. To indicate the accuracy of the simulations let us mention that the vesicle surface is conserved within a relative error of 10^{-6} and local contour length within 10^{-3}.

The normal stress difference is defined as $N = \sigma_{xx} - \sigma_{yy}$, where $\boldsymbol{\sigma}$ is the stress tensor of the suspension, computed using [18,19]:

$$N = \frac{1}{A\eta_0\dot{\gamma}}\left[\oint_\gamma (xf_x - yf_y)ds + 2\eta_0(\lambda - 1) \times \oint_\gamma (n_x v_x - n_y v_y)ds\right]. \qquad (3)$$

The x, y coordinate system is relative to the instantaneous vesicle position and is defined in Fig. 2. The coordinate axes correspond to circumferential and radial directions ($\mathbf{e}_\theta$, $-\mathbf{e}_r$) and the origin is at the vesicle's center of mass. A is the vesicle area and $\dot{\gamma} = -2a/r^2$ the imposed shear rate. Notice that it depends on the radial position of the vesicle.

Description of the numerical experiments.—First, we consider a single two-dimensional vesicle immersed in a Newtonian fluid with a velocity field $v_\theta = a/r$, $v_r = 0$ (for a Couette flow, $v_\theta = a/r + br$). This is an unbounded flow. This choice is made in order to exclude any migration due to bounding walls, allowing us to identify the role of curvature in the flow lines. Boundaries are introduced in a second step. Vesicles are initialized at a distance of $10r_0$ from the origin, where $r_0 = \sqrt{A/\pi}$. The length unit is chosen to be r_0 in our simulations. The dimensionless numbers that enter the problem are [20] the reduced vesicle area $\alpha = \sqrt{A/[\pi(p/2\pi)]^2}$, the viscosity contrast λ, and the capillary number $C_a = \eta_0\dot{\gamma}r_0^3/\kappa$. In the simulations both α and λ are varied. The value of C_a depends on the radial position (varying from $C_a = 0.2$ for $r/r_0 = 10$ to $C_a \approx 2.2$ for $r/r_0 = 3$), while a is fixed to a value $a = -10$ (a weak dependence of vesicle dynamics on this parameter [17] is observed). We have performed three sets of simulations for different $\alpha \in \{0.7; 0.8; 0.9\}$. For every set the range $\lambda \in [1, 10]$ is explored, a range that covers both tank-treading and tumbling regimes [11,17,21].

Results.—Typical simulation results are shown in Fig. 1. Tank-treading vesicles migrate towards the center, while tumbling ones show a negligibly small outward migration. We have found that the migration rate depends on the reduced area and viscosity contrast in a nontrivial way. In Fig. 3, we report the migration velocity v^{mig} for different vesicles at fixed initial radial position $r = 10r_0$. Analogous results are obtained for any radial position $3 \leq r/r_0 \leq 10$. In the left panel, the migration velocity is shown as a function of the two independent dimensionless parameters explored in our simulations, namely, (α, λ).

The data do not seem to show a simple trend. For example, the lines in Fig. 3(a) for migration velocities obtained for different vesicles intersect at some viscosity contrast. This points to the absence of a simple law in this parameter space. We have thus attempted to rationalize these results by evoking basic physical facts that distinguish a simple fluid from a complex one. A particular

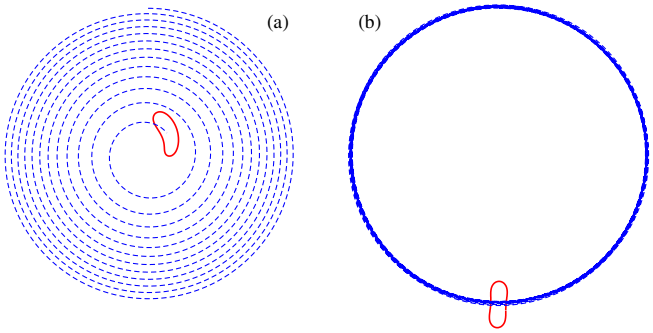

FIG. 1 (color online). Trajectory and contour of (a) tank-treading vesicle ($\alpha = 0.7$, $\lambda = 1$) migrating towards high shear regions and (b) tumbling vesicle ($\alpha = 0.7$, $\lambda = 4$) showing no significant radial migration (after 13 revolutions and 8 tumbling periods).

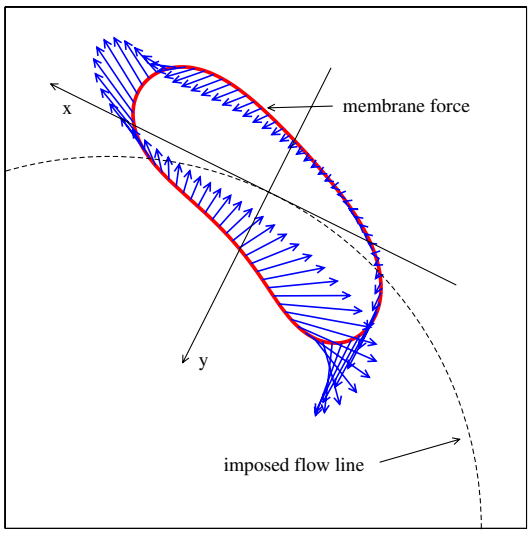

FIG. 2 (color online). Force distribution on vesicle membrane from Eq. (2) and local coordinate system used for the calculation of N ($\alpha = 0.7$, $\lambda = 1$).

2

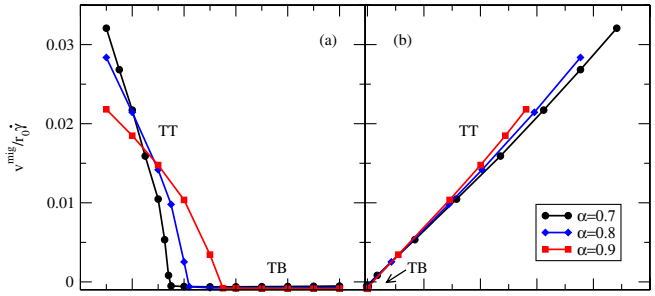

FIG. 3 (color online). Inward migration velocity normalized by $r_0\dot{\gamma}$ as a function of (a) λ and (b) N for different α at fixed radial position $r = 10r_0$. Every point corresponds to the (λ, N) pair on the abscissas.

property of complex fluids is the manifestation of normal stress difference. We have thus represented the data [Fig. 3(b)], in terms of the normal stress difference N measured in the (x, y) coordinate system (see Fig. 2 for notations). Interestingly enough, we observe that the data closely collapse on a single master curve, showing that the dynamics does not depend on the control parameters (α, λ) independently, but rather on their combination embedded in the function $N(\alpha, \lambda)$. Moreover, Fig. 3(b) shows that $v^{\mathrm{mig}}/r_0\dot{\gamma}$ is simply proportional to N. This result holds for all the radial positions explored so far, $3 \leq r/r_0 \leq 10$: data collapse is manifested within an error of 10% (or less), and the results are represented with a universal straight line passing through the origin. The small discrepancies are believed to be due to the details of the flow around vesicles with different shapes and orientations.

To gain further insight we have examined the migration velocity as a function of the curvature of the flow. Figure 4(a) shows $v^{\mathrm{mig}}/Nr_0\dot{\gamma}$ as a function of the radial position. This dependence on r is nonlinear. Expressing the results with the help of an appropriate rescaling [Fig. 4(b)] reveals that $v^{\mathrm{mig}}/N\dot{\gamma}$ is a simple linear function of $\xi \equiv 1/(r/r_0 - 1)$. Note that, approximately, ξ is the flow curvature on the innermost part of the vesicle, which is also the highest among the flow lines passing through the vesicle.

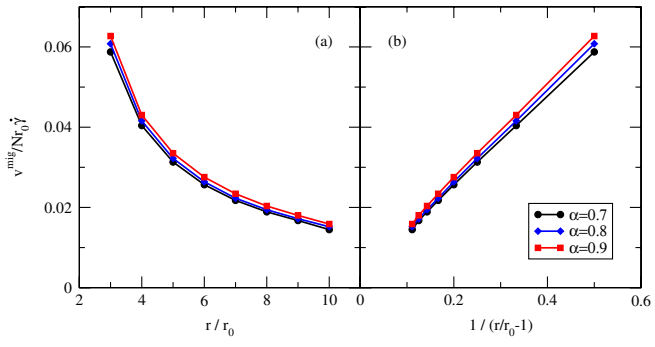

FIG. 4 (color online). Inward migration velocities divided by $Nr_0\dot{\gamma}$ as a function of (a) r and (b) $1/(r - r_0)$ for different α. Every point corresponds to the (λ, N) pair on the abscissas.

This is considered to be due to membrane incompressibility, that propagates stresses along the surface of the vesicle. From the above analysis, we infer the following scaling relation for migration:

$$v^{\mathrm{mig}} \sim r_0\dot{\gamma}\xi N. \tag{4}$$

This is a key result: a macroscopic measure of N (which may be a very complex function of various parameters) directly leads to the determination of the (microscopic) migration velocity. One might ask why should migration be dictated by normal stress difference at all. To answer this question, one may consider the composite fluid and denote its spatial and temporal averaged stress by $\boldsymbol{\sigma}$ [very much like the definition of the classical stress, as used in Eq. (3)]. Let us assume stationary, circular motion, enjoying symmetry with respect to the angle θ. Using momentum conservation in polar coordinates one can show that [22]:

$$\frac{\partial\sigma_{rr}}{\partial r} = \frac{1}{r}[-\rho v_\theta^2 + N], \tag{5}$$

where ρ is the fluid density, $N = \sigma_{\theta\theta} - \sigma_{rr}$, $1/r$ the flowline curvature, and $-\rho v_\theta^2/r$ is the inertia term, which is absent in our case. If $N \neq 0$, a radial stress gradient takes place, resulting in an inward force pushing the fluid towards the center if $N > 0$. No such simple result holds in flows which do not exhibit flowline curvature. This result shows that both N and the flow curvature cause inward motion, in accord with Eq. (4). We have performed simulations in a parallel flow having the same velocity profile as the irrotational vortex, that is $v_x(y) = 1/y$ [in Cartesian coordinates (x, y)]. Contrary to the Couette flow, in parallel flow vesicles migrate toward regions of low shear rate despite the fact that $N > 0$. This points to the conclusion that inward migration in the Couette setup is due to the curvature of the flow lines rather than to a shear gradient.

Tank-treading vesicles show positive normal stresses and they migrate inwards. In the tumbling regime, we have found $N \simeq 0$ (averaged over a tumbling period), and a negligibly small migration. Moreover, N vanishes for tank-treading vesicles when approaching the transition to tumbling or when the shape is close to a sphere [17,23]. This is consistent with the fact that $v_{\mathrm{mig}} \to 0$ with increasing λ or α (Fig. 3).

Having identified the basic phenomena for migration of a single vesicle, we are now in a position to address the question of the impact of this feature on the organization of a collection of vesicles. Here we address the case of a sufficiently dilute suspension. In these simulations we have included confining boundary conditions [14,24], in order to address a realistic situation. Starting from various initial configurations (including a disordered one) we have found that the mutual interactions between vesicles lead to a nontrivial spatial organization. We present the results for a volume concentration $\phi \approx 2\%$ in Fig. 5 (we have

3

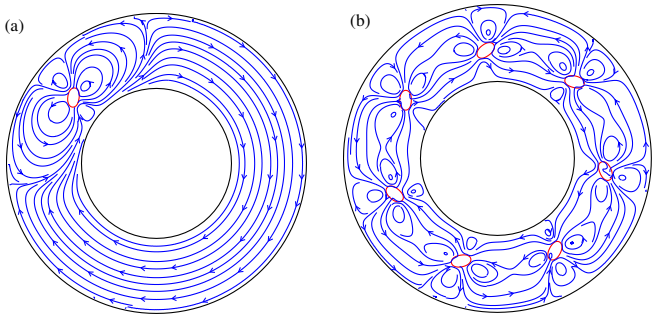

FIG. 5 (color online). Equilibrium configurations in a Taylor-Couette device for (a) a single vesicle and (b) several vesicles (volume fraction $\approx 2\%$). The lines represent the induced flow. Spontaneous organization in (b) is due to inward migration and vortex interaction.

performed simulations with concentrations between $1\% \lesssim \phi \lesssim 6\%$, leading to the same conclusion). After a transient the vesicles exhibit a spatial order: they organize themselves in a rim by keeping the same interdistance. The rim radius is (within numerical uncertainties) very close to the final position of a single vesicle (Fig. 5). A single vesicle stops when the inward migration compensates the lift force due to the inner cylinder. The organization in a rim which has the same radius as that dictated by the final position of a single vesicle is not obvious: indeed, the fact that the vesicles select the same interdistance is a clear indication for their significant mutual interactions, and despite this effect the terminal position does not seem to be affected.

For a better understanding, we have analyzed the behavior of the flow lines. A single vesicle creates two vortices as shown in Fig. 5(a). The size of the vortices is of about a quarter of the circumference. We thus expect vesicles to interact significantly when their number M approaches 4. This is confirmed by our simulations that show disorder for $M < 4$ and order for $M \geq 4$. For $M \geq 4$ vesicles keep order because deviations would cause restoring forces due to vortex interactions. For all explored volume fractions we found persistence of order as shown in Fig. 5(b).

Finally, in view of the generality of the arguments presented for migration, it is natural to attempt to extend them to other types of complex fluids. For example, experimental measurements of migration are known for soft entities in Taylor-Couette and cone-plate rheometers: drops [5,25,26] and polymers in dilute suspensions [27,28] either migrate towards the center (cone plate) or adopt an equilibrium position that lies between the gap center line and the inner cylinder (Taylor-Couette), which corresponds to high shear rate regions. Because drops, polymers, and vesicles have quite different properties, their similar behavior with respect to migration supports our conjecture that the basic mechanisms governing migration are independent of the mechanical details of the suspended entity and depend only on the flow curvature and N. An interesting line of research would be to study the evolution of order for higher concentrations, and provide a detailed link between microstructure and rheology.

C. M. acknowledges financial support from CNES and ANR MOSICOB. G. B. and A. R. were supported by the U.S. National Science Foundation OCI-1047980 and OCI-0923710.

[1] P. Coussot, J. S. Raynaud, F. Bertrand, P. Moucheront, J. P. Guilbaud, H. T. Huynh, S. Jarny, and D. Lesueur, Phys. Rev. Lett. **88**, 218301 (2002).
[2] G. K. Batchelor and J. T. Green, J. Fluid Mech. **56**, 375 (1972).
[3] S. Wu, Polym. Eng. Sci. **19**, 638 (1979).
[4] R. H. Shafer, N. Laiken, and B. H. Zimm, Biophys. Chem. **2**, 180 (1974).
[5] P. C. H. Chan and L. G. Leal, J. Fluid Mech. **92**, 131 (1979).
[6] O. B. Usta, J. E. Butler, and A. J. C. Ladd, Phys. Rev. Lett. **98**, 098301 (2007).
[7] T. W. Secomb, B. Styp-Rekowska, and A. R. Pries, Ann. Biomed. Eng. **35**, 755 (2007).
[8] B. Kaoui, G. H. Ristow, I. Cantat, C. Misbah, and W. Zimmermann, Phys. Rev. E **77**, 021903 (2008).
[9] S. K. Doddi and P. Bagchi, Int. J. Multiphase Flow **34**, 966 (2008).
[10] J. A. Hanna and P. M. Vlahovska, Phys. Fluids **22**, 013102 (2010).
[11] S. R. Keller and R. Skalak, J. Fluid Mech. **120**, 27 (1982).
[12] M. Kraus, W. Wintz, U. Seifert, and R. Lipowsky, Phys. Rev. Lett. **77**, 3685 (1996).
[13] V. Kantsler and V. Steinberg, Phys. Rev. Lett. **95**, 258101 (2005).
[14] A. Rahimian, S. K. Veerapaneni, and G. Biros, J. Comput. Phys. **229**, 6466 (2010).
[15] W. Helfrich, Z. Naturforsch. **28**, 693 (1973).
[16] U. Seifert, Eur. Phys. J. B **8**, 405 (1999).
[17] G. Ghigliotti, T. Biben, and C. Misbah, J. Fluid Mech. **653**, 489 (2010).
[18] G. K. Batchelor, J. Fluid Mech. **41**, 545 (1970).
[19] M. R. Kennedy, C. Pozrikidis, and R. Skalak, Comput. Fluids **23**, 251 (1994).
[20] B. Kaoui, A. Farutin, and C. Misbah, Phys. Rev. E **80**, 061905 (2009.
[21] J. Beaucourt, F. Rioual, T. Séon, T. Biben, and C. Misbah, Phys. Rev. E **69**, 011906 (2004).
[22] R. B. Bird, R. C. Armstrong, and O. Hassager (John Wiley and Sons Inc., New York, NY, 1987).
[23] G. Danker and C. Misbah, Phys. Rev. Lett. **98**, 088104 (2007).
[24] S. K. Veerapaneni, D. Gueyffier, D. Zorin, and G. Biros, J. Comput. Phys. **228**, 2334 (2009).
[25] P. C.-H. Chan and L. G. Leal, Int. J. Multiphase Flow **7**, 83 (1981).
[26] K. G. Hollingsworth and M. L. Johns, J. Colloid Interface Sci. **296**, 700 (2006).
[27] P. O. Brunn, J. Chem. Phys. **80**, 3420 (1984).
[28] M. V. Apostolakis, V. G. Mavrantzas, and A. N. Beris, J. Non-Newtonian Fluid Mech. **102**, 409 (2002).

4